ARCSC-Net: An Approximate Residual Convolutional Sparse Coding Network For Compressed Sensing MRI

Qian Wang[1]
wang_qian@stumail.ysu.edu.cn

Pengyu Li[1]
pyli80@163.com

Jinjia Wang[1,2]
wjj@ysu.edu.cn

[1] School of Information Science and Engineering
Yanshan University
Qinhuangdao, Hebei Province, Peoples Republic of China

[2] Hebei Key Laboratory of Information Transmission and Signal Processing
Yanshan University
Qinhuangdao, Hebei Province, Peoples Republic of China

Abstract

Compression sensing magnetic resonance imaging (CS-MRI) provides a theoretical basis for reducing magnetic resonance (MR) data acquisition time and accelerating the imaging process. In recent years, the CS-MRI algorithm based on deep learning has attracted significant attention and developed rapidly in theoretical research. However, the compression sensing based methods do not capture the detail component of an image very well. Inspired by this, we propose an improved learning iterative shrinkage-thresholding algorithm for convolutional sparse coding (CSC) and unfold it with neural networks, named an approximate residual convolutional sparse coding network (ARCSC-Net). The new network improves learning ability and efficiency to capture the high-frequency details of the image compared to other algorithms. Firstly, unlike the traditional CSC algorithms, we relax the constraints on a single convolutional dictionary and extract higher-level detail features using multiple iterative layers corresponding to different convolutional dictionaries. Secondly, we add residual structures to the network to preserve the low-frequency MR images of under-sampled *k*-space data. Thirdly, we introduce the data consistency layer to enhance the fidelity of the *k*-space data, thereby improving the reconstruction performance of the network. Experimental results show that ARCSC-Net is superior to the state-of-the-art CS-MRI methods in terms of runtime and reconstructed image quality.

1 Introduction

Magnetic resonance imaging (MRI) is an important diagnostic method in the medical field [1, 19, 39]. It is popular for achieving high-resolution images and providing clinicians

with rich diagnostic information. In addition, the technique does not produce ionizing radiation on the patients during clinical examinations. However, the imaging speed of MRI is slow and usually takes a lot of scanning time to produce high-quality images. Therefore, it is necessary to reduce scanning time without sacrificing image quality using fast MRI technology.

Compression sensing (CS) is an effective method for fast MRI [9, 10]. It is designed to reconstruct MR images from under-sampled k-space data that is much less than Nyquist sampling, using prior information such as sparseness [5, 17], local or non-local similarity of images [8, 27], or low rank [13, 18]. For compression sensing magnetic resonance imaging (CS-MRI), the key to improving the reconstruction performance is the sparse regularization associated with data a priori. Traditional CS-MRI methods typically explore sparse regularization in specific transformation domains [7, 12, 20, 22] or dictionary-based subspaces [3, 4, 15, 21]. However, these methods cannot meet the requirements of MRI reconstruction in both running time and reconstruction performance.

Recently, deep learning has made encouraging achievements in some tasks, such as image classification [33, 37] and medical image reconstruction [24, 29]. Inspired by this, many studies have applied deep learning to MRI reconstruction and achieved significant performance gains [16, 28, 30, 31, 34, 35, 36, 38]. These methods can be divided into two categories. The first category directly uses neural networks to end-to-end learn the mapping between zero-filled reconstruction images and fully-sampled reconstruction images [28, 31, 34, 35]. The second category combines the advantages of model-driven and data-driven methods to build iterative neural networks by combining forward neural networks with traditional iterative algorithms [16, 30, 36, 38].

Inspired by unfolding iterative algorithms, we propose an iterative neural network based on convolutional sparse coding (CSC) for CS-MRI.

The main contributions of our work are as follows.

• Based on the iterative shrinkage-thresholding algorithm (ISTA) for the CSC problem, we propose an improved learning ISTA.

• Based on the proposed learning ISTA, we propose an approximate residual convolutional sparse coding network (ARCSC-Net) for CS-MRI.

The remainder of this article is organized as follows. Section 2 describes the proposed algorithm and network. The experiments and results are presented in Section 3. The final section concludes this paper.

2 Proposed method

2.1 Improved learning ISTA for CSC

In this section, we first briefly review the general CS-MRI model and the theoretical knowledge of CSC, then detail the proposed improved learning ISTA for CSC.

2.1.1 The CS-MRI Model

Assume $x \in C^N$ is an MR image to be reconstructed, $y \in C^M$ $(M < N)$ is the under-sampled k-space data. The general CS-MRI model can be described as:

$$\hat{x} = \arg\min_x \left\{ \frac{1}{2} \|y - F_u x\|_2^2 + \lambda \|\Psi x\|_1 \right\} \tag{1}$$

where F_u is an under-sampled Fourier transform matrix, Ψ is a sparse transformation mapping matrix. In Eq. (1), the former is the data fidelity term, and the latter is the regularization term. λ is the regularization parameter that balances the two terms.

2.1.2 Convolution sparse coding

It is a classical approach to split the signal into patches and solve sparse coding (SC) separately:

$$\min \|z\|_1 \quad s.t. x = Dz \tag{2}$$

where $z \in R^m$ is the sparse representation of $x \in R^n$ under over-complete dictionary $D \in R^{n \times m}$. However, it takes a significant amount of time to solve SC on all patches. Due to shift-invariance in images [32], learning the dictionary independently on each patch will lose its external spatial information.

CSC is adopted to apply additional prior knowledge based on the entire signal [14, 23]. CSC uses the convolutional dictionary:

$$\arg\min_z \frac{1}{2} \|x - Dz\|_2^2 + \lambda \|z\|_1 . \tag{3}$$

A popular technique to minimize Eq. (3) is the ISTA [6] iteration:

$$z_k = S_\theta \left(z_{k-1} + D^T \left(x - Dz_{k-1} \right) \right), \quad k = 1, \cdots, K, \tag{4}$$

where K is the maximum value, and S_θ is the soft-thresholding operator that is expressed as

$$S_\theta(x) = sign(x) \, max(|x| - \theta, 0). \tag{5}$$

Moreover, Sreter and Giryes [32] proposed approximate convolutional sparse coding (ACSC) for image denoising. ACSC learns the convolution dictionary and minimizes Eq. (3) by Eq. (6)

$$z_k = S_\theta \left(z_{k-1} + D_e^T \left(x - D_d z_{k-1} \right) \right), \tag{6}$$

where D_e and D_d are different convolution dictionaries.

2.1.3 Improved learning ISTA for CSC

The ISTA is a classic method for solving linear inverse problems. This section proposes improvements to the learning ISTA for CSC in [32]. The CSC model is suitable for high-frequency modeling components [11]. Unlike the CSC model acting on the whole image [32], we divide the image into two parts: the low-frequency and high-frequency components. We use the zero-filling MR image x_0 as the low-frequency component. We use the CSC model to capture the image detail information and reconstruct the high-frequency components from the original input signal x_0. The algorithm first uses the CSC to obtain the initial sparse coefficient of x_0, then uses ISTA to update the sparse coefficient, and then uses the convolutional dictionary D to decode the z_K and obtain the reconstructed high-frequency components. Finally, it is superimposed with x_0 to get a complete reconstructed image $\hat{x}$. The iterative steps are as follows:

$$z_0 = D_e^T x_0, \tag{7}$$

$$z_k = S_\theta \left(z_{k-1} + D_e^T \left(x_0 - D_d z_{k-1} \right) \right), \quad k = 1, \cdots, K, \tag{8}$$

$$\hat{x} = Dz_K + x_0, \tag{9}$$

where z_k and z_{k-1} represent the sparse coefficient of the current and previous iteration, respectively. S_θ is the soft-thresholding operator, and $D_e^T(x_0 - D_d z_{k-1})$ represents the error correction term. The ISTA algorithm minimizes the error correction term as much as possible in each iteration, updating the sparse coefficient of this iteration to make it better than the result of the previous iteration.

We summarize the improved learning ISTA for CSC in **Algorithm 1**.

Algorithm 1 Improved learning ISTA for CSC

Input: original signal x_0

Initialization: $D_e, D_d, D, z_0 = D_e^T x_0$

    for iteration $k = 1 : K$ **do**

        Update z_k of the current iteration using Eq.(8)

    end for

    Reconstruct signal $\hat{x}$ via Eq.(9)

Output: The final sparse coding z_K, the reconstructed signal $\hat{x}$

2.2 Proposed ARCSC-Net

In this section, we first outline the overall architecture of the proposed ARCSC-Net, then describe its critical components in detail.

2.2.1 ARCSC-Net for CS-MRI
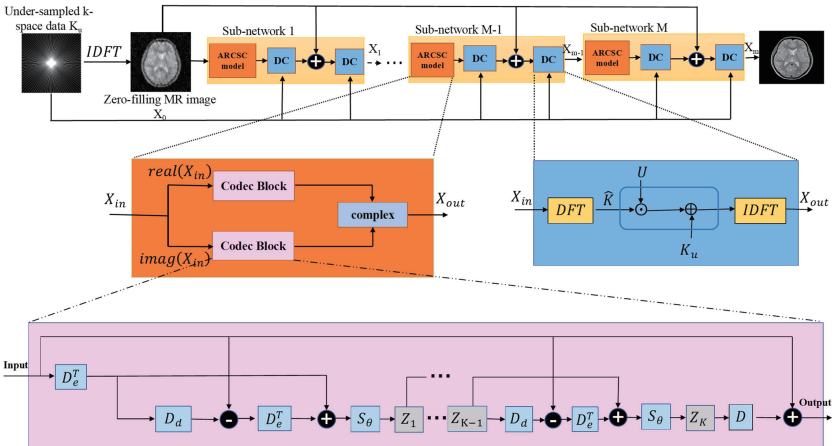
Figure 1: The architecture of ARCSC-Net. There are M sub-networks, each of which includes the ARCSC model and data consistency(DC) layer.

The proposed ARCSC-Net for CS-MRI is shown in Figure 1. It consists of a series of cascading sub-networks, each containing an ARCSC model and two DC layers. The ARCSC model first decomposes the input complex data into real and imaginary parts, then encodes and decodes them respectively, and finally synthesizes the decoding results to obtain the reconstructed complex image. The DC layer improves the fidelity of the input image corresponding to the k-space data in the model.

First, a zero-filling MR image $X_0 = IDFT(K_u)$ is generated from under-sampled k-space data K_u, which is then fed into a series of cascading sub-networks for reconstruction. We represent the reconstructed MR image as $\hat{X}$ and the entire network model as $f(.)$. Assuming that the proposed ARCSC-Net has M sub-networks, the m-th $(1 \leq m \leq M)$ sub-network outputs the current prediction X_m based on the output X_{m-1} of the previous iteration and the input X_0 of the network. X_m can be expressed as:

$$X_m = f_m(X_0, X_{m-1}) \tag{10}$$

where f_m represents the operation of the m-th sub-network, the final reconstructed MR image can be described as:

$$\hat{X} = f_M(X_0, X_{M-1}) \tag{11}$$

2.2.2 ARCSC-model

The ARCSC model contains two sub-modules (Codec block) with the same structure, which process the real and imaginary parts of the input data. The codec block is the core of the ARCSC model. The key for the codec block to learning input data features is the excellent performance of convolutional dictionaries in extracting features. As shown in the pink part of Figure 1, the codec block adopts ARCSC-Ne to obtain an accurate sparse coding, then decodes the sparse coding to get a reconstructed signal, and adds the reconstructed signal with the input signal to form the image domain residual structure. This will further deepen our network.

2.2.3 Residual structure

With the deepening of network construction, the redundancy of some features information in the model increases, which may lead to the overall network losing sensitivity to the details of the image outline in the learning process, thereby restricting network performance. We introduce a residual structure in ARCSC-Net so that each level of the sub-network not only connects to the output of the previous sub-network but also receives the input under-sampled MR image. To a certain extent, it enhances the feature learning ability of the subsequent sub-networks, solves the problem of increasing the redundancy of feature information in the network, delays the gradient disappearance problem, and makes the loss function guiding the network training converge faster and better, thereby further improving the reconstruction performance of the overall network.

2.2.4 Relax convolutional dictionary constraints

Unlike the single convolutional dictionary used in the MRI under-sampling reconstruction network based on CSC, ARCSC-Net relaxes the constraint restrictions on the CSC single dictionary, using multiple convolutional layers corresponding to different convolutional dictionaries D_d and D_e, and completing the codec process in a manner that ACSC. ARCSC-Net

uses multi-layer convolution to extract higher-level features and obtain richer information, which is of great help in improving the performance of network reconstruction.

2.2.5 Data consistency layer

ARCSC-Net uses the DC layer across multi-level sub-networks to implement constraints on k-space data. The DC module in Figure 1 is the data consistency layer, and its internal structure is shown in the blue part of Figure 1. It updates X_{in} to X_{out} according to the fidelity of the data in the k-space as follows.

$$X_{\text{out}} = \text{dc}(X_{\text{in}}, K_u) = \text{idft}(\hat{K} \odot U + K_u) \tag{12}$$

where dft represents a 2D discrete Fourier transform (DFT) and idft is a 2D inverse discrete Fourier transformation (IDFT). K_u represents known under-sampled k-space data, U is the sampling matrix, and $\hat{K}$ represents the k-space data corresponding to the reconstructed image.

2.2.6 Network training

During training, we consider the data loss of both the image space domain and the k-space domain and use the MSE and MAE weighted combination method to construct the loss function of the network. We set the weight of the MSE to 0.2 and the weight of the MAE to 0.8. We minimized the loss function through the Adam optimizer.

3 Experiments and results

In this section, we conduct extensive experiments to evaluate the reconstruction performance of ARCSC-Net proposed in this paper.

3.1 Implementation details

We train and test ARCSC-Net on brain and knee datasets. We randomly select 100 images of each dataset for training and another 100 for testing. The pseudo-radial sampling scheme shown in Figure 2 is used in the experiment to learn ARCSC-Net for various sampling rates. We set the convolutional kernel size of the convolutional layer to 3×3, the step size to 1, the convolutional layer filter to 64, and the additional activation function to the ReLU function. Each sub-network iterates over the input image data into real and imaginary parts. The Adam optimizer trains the network to achieve gradient descent and backpropagation. The learning rate is initialized to 2×10^{-4}. The model uses the TensorFlow framework and is trained on a GPU with NVIDIA GTX 1080 Ti.

To evaluate the performance of ARCSC-Net proposed in this paper, we compare it to five state-of-the-art CS-MRI methods, namely SIDWT [2]; PBDW [25]; PANO [26]; ReconGAN [28]; RefineGAN [28]. All the code for the above comparison experiments is downloaded from the author's website and reproduced strictly following the original paper.

In order to quantitatively evaluate the reconstruction performance of various methods, the peak signal-to-noise ratio (PSNR) and structural similarity index measure (SSIM) are used as objective evaluation indicators of experimental results.

| (a) 30% | (b) 40% | (c) 50% | (d) 60% |
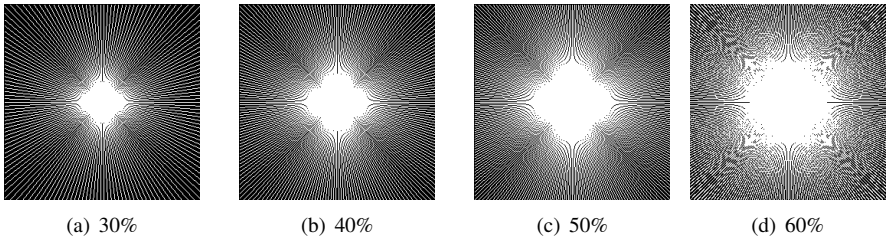
Figure 2: Pseudo radial sampling masks used in our experiments.

3.2 The impact of the number of sub-networks and the number of iteration layers

Figure 3 and Figure 4 show the quantitative results of reconstructing brain images using ARCSC-Net under a 30% pseudo-radial sampling pattern, the number of iteration layers is 20, a different number of sub-networks, and 30% pseudo-radial sampling pattern, the number of sub-networks is 3, and different iteration layers, respectively. It can be seen that both the PSNR and SSIM of the reconstructed image increase with the increase in the number of sub-networks and iteration layers. In Figure 3, as the number of iterations increases, the PSNR value increases by about 3dB and the SSIM value increases by about 0.008 as M increases from 1 to 3. In Figure 4, as the number of iterations increases, the PSNR value increases by approximately 0.5dB and the SSIM value by about 0.0008 as the number of iteration layers increases from 3 to 20. In particular, when the number of sub-networks M and the number of iteration layers reaches 3 and 20, respectively, the performance of ARCSC-Net reaches saturation. Therefore, within a specific range, the increase of parameter M and the number of iteration layers can improve the reconstruction performance of the network. In addition, in subsequent experiments, we set the default values for M and the number of iteration layers to 3 and 20, respectively.
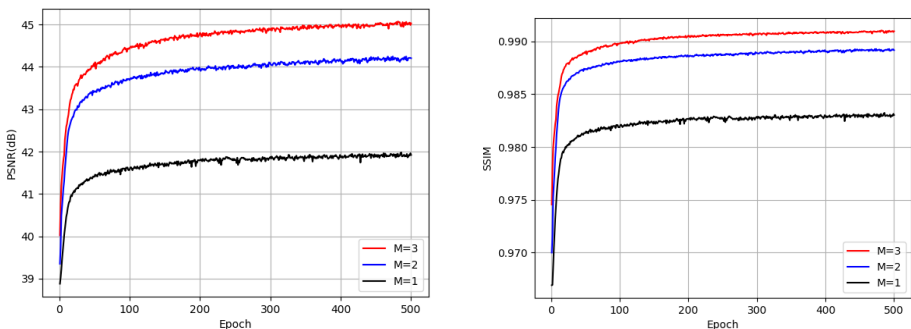
Figure 3: M vs PSNR(left) M vs SSIM(right).

3.3 Comparison with other advanced CS-MRI methods

Figure 5 and Figure 6 show the quantitative results of different methods at different sampling rates using a pseudo-radial sampling scheme. We can see that the proposed ARCSC-
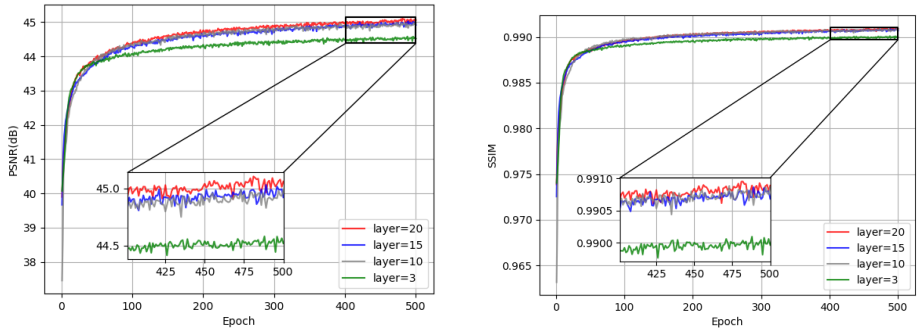
Figure 4: layer vs PSNR(left) layer vs SSIM(right).

Net reconstructs the most accurate results compared with other methods. ARCSC-Net based on CSC has excellent performance for high-frequency image reconstruction. With the increase of the sampling rate, the high-frequency information contained in the under-sampled images increases, and the high-frequency details of the images are gradually enriched. Thus, the quality of the images reconstructed by ARCSC-Net is much better than that of other methods under the same sampling rate. At a sampling rate of 30%, ARCSC-Net obtains performance improvement at least 5.5dB higher in PSNR than other methods. When the sampling rate reaches 60%, the PSNR of the reconstructed images by ARCSC-Net is at least 7.5dB higher than that of other methods. In addition, the images reconstructed by ARCSC-Net have higher SSIM and smaller variance. Compared with other methods, ARCSC-Net has higher structural stability.

(a) 30%   (b) 40%   (c) 50%   (d) 60%
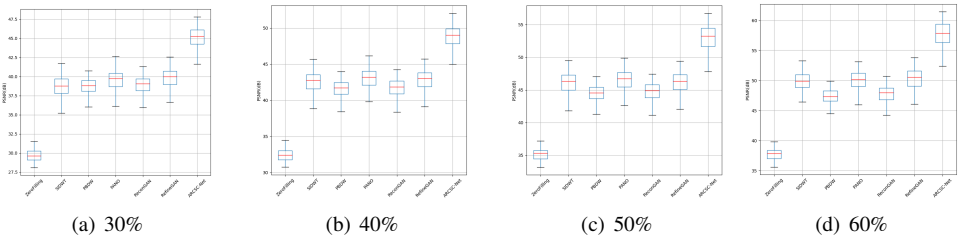
Figure 5: PSNR evaluations on the brain test set.

(a) 30%   (b) 40%   (c) 50%   (d) 60%
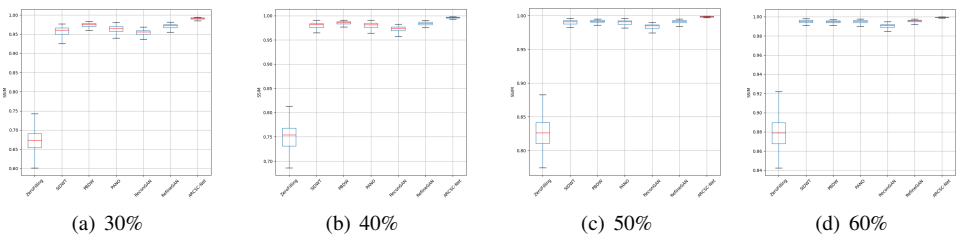
Figure 6: SSIM evaluations on the brain test set.

Figure 7 and Figure 8 show a visual comparison of brain data at 30% and 40% sampling rates. It is worth noting that in Figure 7 and Figure 8, the color range of the error image in the second row is [0,40] and [0,25], respectively. With the increase in sampling rate, the error of the under-sampled image decreases. Different methods are used to reconstruct the under-sampled image, and the error of the reconstructed image is less than that of the under-sampled image. From all the corresponding error images of reconstructed images, we can see that our proposed ARCSC-Net obtains the highest-quality images with the minimum reconstructed error.
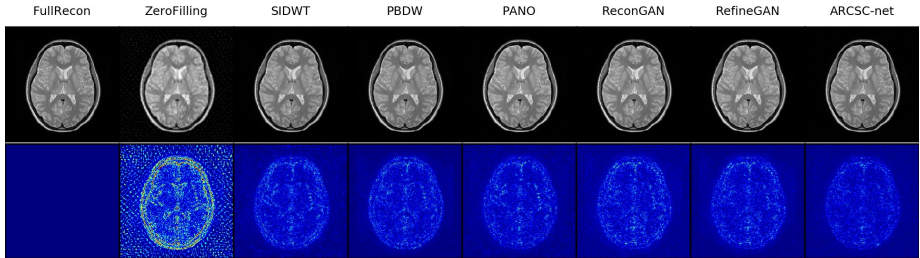
Figure 7: Results on brain MR images using 30% pseudo radial undersampling.
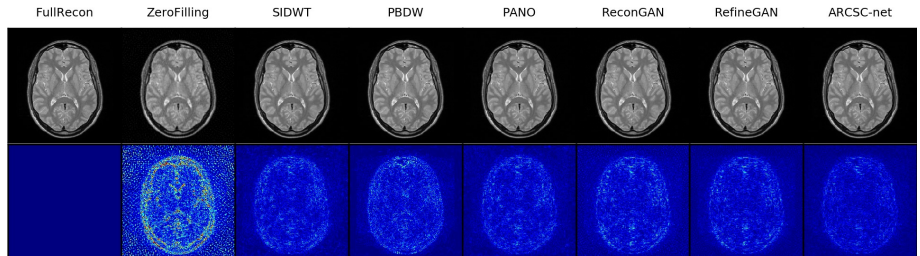
Figure 8: Results on brain MR images using 40% pseudo radial undersampling.

We further investigated the performance of ARCSC-Net to reconstruct knee data. The sampling pattern used in the experiment is pseudo-radial, with a sampling rate of 30%. The visualization results are shown in Figure 9, and the color range of the error image in the second row is [0,30]. It can be observed that our proposed ARCSC-Net can reconstruct the image details more accurately with the minimum reconstruction error. Knee data are complex-valued data with less detailed information than brain data. In the reconstruction of knee images, CSC can not give full play to its advantages of learning high-frequency details. The CSC-based method can better reconstruct MR images with more high-frequency information.

To demonstrate the ability of the ARCSC-Net to handle noise. We add Gaussian white noise with a standard deviation of 0.015 to the real and imaginary parts of the original k-space data. The reconstruction performance of different methods in noise conditions is investigated under a pseudo-radial sampling scheme of 30%. In contrast, other methods are dramatically affected by noise. Our ARCSC-Net yields superior or comparable reconstruction results with other CS-MRI methods using pseudo-radial sampling schemes.

| FullRecon | ZeroFilling | SIDWT | PBDW | PANO | ReconGAN | RefineGAN | ARCSC-net |
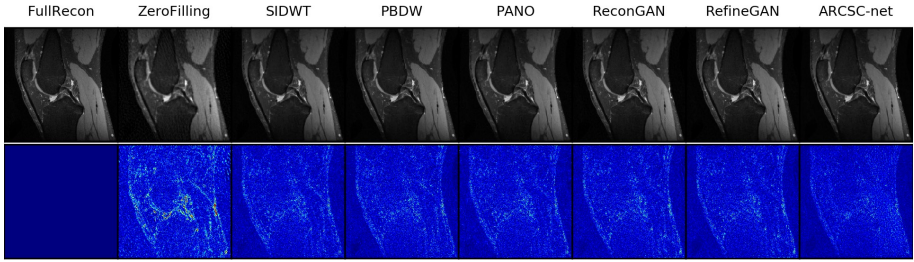
Figure 9: Results on knee MR images using 30% pseudo radial undersampling.

3.4 Runtime

In this section, we compare the runtime of ARCSC-Net with other advanced CS-MRI methods. As shown in Table 1, deep learning-based ReconGAN, RefineGAN, and ARCSC-Net run in less than a second, far shorter than CPU-dependent SIDWT, PBDW, and PANO. At GPU acceleration, neural network-based models are reconstructed much faster than non-neural network methods. Experiments have shown that ARCSC-Net has better reconstruction performance without significantly increasing runtime.

Table 1: Running time comparison of different methods on brain datasets using 10% pseudo radial mask.

Methods	SIDWT	PBDW	PANO	ReconGAN	RefineGAN	ARCSC-Net
Times(seconds)	22.32814	98.48442	23.51991	0.06075	0.10615	0.11341

4 Conclusion

In this paper, we propose an improved learning ISTA for CSC and expand it into a novel CS-MRI deep network called ARCSC-Net. The proposed ARCSC-Net combines the advantages of traditional iterative algorithms and deep neural networks, which has good interpretability and excellent reconstruction performance. We compared it with the state-of-the-art CS-MRI methods on brain and knee images. Numerous experiments have shown that our network performs better in quantitative comparison and visual quality. In the future, we will study the optimization algorithm of the CSC model under the constraints of the l_0 norm and unroll it to an iterative neural network.

Acknowledgements

References

[1] Md Zahangir Alom, Lili He, Tarek M Taha, and Vijayan K Asari. Fast and accurate magnetic resonance image (mri) reconstruction with nabla-n network. In *Applications of Machine Learning 2020*, volume 11511, pages 50–58. SPIE, 2020.

[2] Richard G. Baraniuk. Compressive sensing [lecture notes]. *IEEE Signal Processing Magazine*, 24(4):118–121, 2007.

[3] Jianxin Cao, Shujun Liu, Hongqing Liu, and Hongwei Lu. Cs-mri reconstruction based on analysis dictionary learning and manifold structure regularization. *Neural Networks*, 123:217–233, 2020.

[4] Shekhar S Chandra, Marlon Bran Lorenzana, Xinwen Liu, Siyu Liu, Steffen Bollmann, and Stuart Crozier. Deep learning in magnetic resonance image reconstruction. *Journal of Medical Imaging and Radiation Oncology*, 65(5):564–577, 2021.

[5] Zhen Chen, Chuanping Huang, and Shufu Lin. A new sparse representation framework for compressed sensing mri. *Knowledge-Based Systems*, 188:104969, 2020.

[6] Ingrid Daubechies, Michel Defrise, and Christine De Mol. An iterative thresholding algorithm for linear inverse problems with a sparsity constraint. *Communications on Pure and Applied Mathematics: A Journal Issued by the Courant Institute of Mathematical Sciences*, 57(11):1413–1457, 2004.

[7] Dong Du, Zhibin Pan, Penghui Zhang, Yuxin Li, and Weiping Ku. Compressive sensing image recovery using dictionary learning and shape-adaptive dct thresholding. *Magnetic resonance imaging*, 55:60–71, 2019.

[8] Ender M Eksioglu. Decoupled algorithm for mri reconstruction using nonlocal block matching model: Bm3d-mri. *Journal of Mathematical Imaging and Vision*, 56(3):430–440, 2016.

[9] Li Feng, Thomas Benkert, Kai Tobias Block, Daniel K Sodickson, Ricardo Otazo, and Hersh Chandarana. Compressed sensing for body mri. *Journal of Magnetic Resonance Imaging*, 45(4):966–987, 2017.

[10] Urs Gamper, Peter Boesiger, and Sebastian Kozerke. Compressed sensing in dynamic mri. *Magnetic Resonance in Medicine: An Official Journal of the International Society for Magnetic Resonance in Medicine*, 59(2):365–373, 2008.

[11] Cristina Garcia-Cardona and Brendt Wohlberg. Convolutional dictionary learning: A comparative review and new algorithms. *IEEE Trans. Comput. Imag.*, 4(3):366–381, 2018. doi: 10.1109/TCI.2018.2840334.

[12] Justin P Haldar and Kawin Setsompop. Linear predictability in mri reconstruction: Leveraging shift-invariant fourier structure for faster and better imaging. *IEEE Signal Process. Mag.*, 2020.

[13] Zhao He, Ya-Nan Zhu, Suhao Qiu, Tao Wang, Chencheng Zhang, Bomin Sun, Xiaoqun Zhang, and Yuan Feng. Low-rank and framelet based sparsity decomposition for interventional mri reconstruction. *IEEE Transactions on Biomedical Engineering*, 2022.

[14] Felix Heide, Wolfgang Heidrich, and Gordon Wetzstein. Fast and flexible convolutional sparse coding. In *Proceedings of the IEEE Conference on Computer Vision and Pattern Recognition*, pages 5135–5143, 2015.

[15] Yue Hu, Xiaohan Liu, and Mathews Jacob. A generalized structured low-rank matrix completion algorithm for mr image recovery. *IEEE transactions on medical imaging*, 38(8):1841–1851, 2018.

[16] Yuxin Hu, Yunyingying Xu, Qiyuan Tian, Feiyu Chen, Xinwei Shi, Catherine J Moran, Bruce L Daniel, and Brian A Hargreaves. Run-up: Accelerated multishot diffusion-weighted mri reconstruction using an unrolled network with u-net as priors. *Magnetic Resonance in Medicine*, 85(2):709–720, 2021.

[17] Zongying Lai, Xiaobo Qu, Yunsong Liu, Di Guo, Jing Ye, Zhifang Zhan, and Zhong Chen. Image reconstruction of compressed sensing mri using graph-based redundant wavelet transform. *Medical image analysis*, 27:93–104, 2016.

[18] Die Liu, Jinjie Zhou, Miaomiao Meng, Fan Zhang, Minghui Zhang, and Qiegen Liu. Highly undersampling dynamic cardiac mri based on low-rank tensor coding. *Magnetic Resonance Imaging*, 89:12–23, 2022.

[19] Qiegen Liu, Qingxin Yang, Huitao Cheng, Shanshan Wang, Minghui Zhang, and Dong Liang. Highly undersampled magnetic resonance imaging reconstruction using autoencoding priors. *Magnetic Resonance in Medicine*, 83(1):322–336, 2020.

[20] Ryan Wen Liu, Quandang Ma, Simon Chun Ho Yu, Kwok Tai Chui, and Naixue Xiong. Variational regularized tree-structured wavelet sparsity for cs-sense parallel imaging. *IEEE Access*, 6:61050–61064, 2018.

[21] Michael Lustig, David Donoho, and John M Pauly. Sparse mri: The application of compressed sensing for rapid mr imaging. *Magnetic Resonance in Medicine: An Official Journal of the International Society for Magnetic Resonance in Medicine*, 58(6):1182–1195, 2007.

[22] Greg Ongie, Sampurna Biswas, and Mathews Jacob. Convex recovery of continuous domain piecewise constant images from nonuniform fourier samples. *IEEE Transactions on Signal Processing*, 66(1):236–250, 2017.

[23] Vardan Papyan, Yaniv Romano, Jeremias Sulam, and Michael Elad. Convolutional dictionary learning via local processing. In *Proceedings of the IEEE International Conference on Computer Vision*, pages 5296–5304, 2017.

[24] Defu Qiu, Lixin Zheng, Jianqing Zhu, and Detian Huang. Multiple improved residual networks for medical image super-resolution. *Future Generation Computer Systems*, 116:200–208, 2021.

[25] Xiaobo Qu, Di Guo, Bende Ning, Yingkun Hou, Yulan Lin, Shuhui Cai, and Zhong Chen. Undersampled mri reconstruction with patch-based directional wavelets. *Magnetic Resonance Imaging*, 30(7):964–977, 2012.

[26] Xiaobo Qu, Yingkun Hou, Fan Lam, Di Guo, Jianhui Zhong, and Zhong Chen. Magnetic resonance image reconstruction from undersampled measurements using a patch-based nonlocal operator. *Medical Image Analysis*, 18(6):843–856, 2014.

[27] Xiaobo Qu, Yingkun Hou, Fan Lam, Di Guo, Jianhui Zhong, and Zhong Chen. Magnetic resonance image reconstruction from undersampled measurements using a patch-based nonlocal operator. *Medical image analysis*, 18(6):843–856, 2014.

[28] Tran Minh Quan, Thanh Nguyen-Duc, and Won-Ki Jeong. Compressed sensing mri reconstruction using a generative adversarial network with a cyclic loss. *IEEE Transactions on Medical Imaging*, 37(6):1488–1497, 2018.

[29] Swati Rai, Jignesh S Bhatt, and Sarat Kumar Patra. An unsupervised deep learning framework for medical image denoising. *arXiv preprint arXiv:2103.06575*, 2021.

[30] Zaccharie Ramzi, GR Chaithya, Jean-Luc Starck, and Philippe Ciuciu. Nc-pdnet: a density-compensated unrolled network for 2d and 3d non-cartesian mri reconstruction. *IEEE Transactions on Medical Imaging*, 2022.

[31] Jo Schlemper, Jose Caballero, Joseph V. Hajnal, Anthony N. Price, and Daniel Rueckert. A deep cascade of convolutional neural networks for dynamic mr image reconstruction. *IEEE Transactions on Medical Imaging*, 37(2):491–503, 2018.

[32] Hillel Sreter and Raja Giryes. Learned convolutional sparse coding. In *2018 IEEE International Conference on Acoustics, Speech and Signal Processing (ICASSP)*, pages 2191–2195. IEEE, 2018.

[33] Okeke Stephen, Mangal Sain, Uchenna Joseph Maduh, and Do-Un Jeong. An efficient deep learning approach to pneumonia classification in healthcare. *Journal of healthcare engineering*, 2019, 2019.

[34] Shanshan Wang, Zhenghang Su, Leslie Ying, Xi Peng, Shun Zhu, Feng Liang, Dagan Feng, and Dong Liang. Accelerating magnetic resonance imaging via deep learning. In *2016 IEEE 13th International Symposium on Biomedical Imaging (ISBI)*, pages 514–517, 2016.

[35] Guang Yang, Simiao Yu, Hao Dong, Greg Slabaugh, Pier Luigi Dragotti, Xujiong Ye, Fangde Liu, Simon Arridge, Jennifer Keegan, Yike Guo, and David Firmin. Dagan: Deep de-aliasing generative adversarial networks for fast compressed sensing mri reconstruction. *IEEE Transactions on Medical Imaging*, 37(6):1310–1321, 2018.

[36] yan yang, Jian Sun, Huibin Li, and Zongben Xu. Deep admm-net for compressive sensing mri. In *Advances in Neural Information Processing Systems*, volume 29. Curran Associates, Inc., 2016.

[37] Jianpeng Zhang, Yutong Xie, Qi Wu, and Yong Xia. Medical image classification using synergic deep learning. *Medical image analysis*, 54:10–19, 2019.

[38] Xiaohua Zhang, Qiusheng Lian, Yuchi Yang, and Yueming Su. A deep unrolling network inspired by total variation for compressed sensing mri. *Digital Signal Processing*, 107:102856, 2020.

[39] Peixian Zhuang, Xiaowen Zhu, and Xinghao Ding. Mri reconstruction with an edge-preserving filtering prior. *Signal Processing*, 155:346–357, 2019.